J Mater Sci (2008) 43:7132–7140
DOI 10.1007/s10853-008-3029-8

# Isotactic and syndiotactic polypropylene/multi-wall carbon nanotube composites: synthesis and properties

**Anton A. Kovalchuk · Vitaliy G. Shevchenko · Alexander N. Shchegolikhin · Polina M. Nedorezova · Alla N. Klyamkina · Alexander M. Aladyshev**

Received: 12 June 2008 / Accepted: 30 September 2008 / Published online: 24 October 2008


**Abstract** Isotactic polypropylene (iPP) and syndiotactic polypropylene (sPP) nanocomposites containing 0.1–3.5 wt.% multi-wall carbon nanotubes (MWCNTs) have been synthesized via in situ polymerization method with the use of $C_2$- and $C_s$- symmetry zirconocenes activated by methylaluminoxane (MAO) in liquid propylene medium. Fracture morphology studies by SEM reveal different MWCNT dispersion efficiency in various polymer matrices, which arises from the catalytic peculiarities of the composite synthesis. Considerable Young's modulus enhancement of iPP and sPP (25–66%) takes place even at low MWCNT loadings (below 0.5 wt.%). The obtained nanocomposites can find use as efficient electromagnetic shielding materials and microwave absorbing filters due to relatively low permittivity values and considerable dielectric losses in microwave range. Calorimetry data demonstrate that MWCNTs exert evident influence as nucleating agents causing the rise of iPP and sPP crystallization temperature. Considerable retardation effect on iPP thermal oxidative degradation has been observed: the temperature of maximal weight loss rate rises by ~52 °C upon incorporating only 1.4 wt.% MWCNTs.

A. A. Kovalchuk (✉) · P. M. Nedorezova · A. N. Klyamkina · A. M. Aladyshev
N.N. Semenov Institute of Chemical Physics of Russian Academy of Sciences, Kosygin Str., 4, Moscow 119991, Russia
e-mail: kovalchuk@chph.ras.ru; a-kov1@yandex.ru

V. G. Shevchenko
N.S. Enikolopov Institute of Synthetic Polymer Materials of Russian Academy of Sciences, Profsoyuznaya Str., 70, Moscow 117393, Russia

A. N. Shchegolikhin
N.M. Emanuel Institute of Biochemical Physics of Russian Academy of Sciences, Kosygin Str., 4, Moscow 119991, Russia

## Introduction

Due to the unique combination of structural, mechanical, electrical, and thermal transport properties of carbon nanotubes (CNTs) [1, 2], a lot of attention is presently focused on the application of CNTs as fillers to improve properties of polymers and obtaining advanced multifunctional composite materials [3, 4]. Amongst a wide variety of commercially important polymers, polyolefins (polypropylene in particular) constitute the family of the most influential and versatile materials due to their attractive set of properties and low cost [5, 6]. Property modification of polypropylene as a large-volume thermoplastic polymer of extremely high commercial importance is a subject of the present work. Enhancement of polypropylene performance by CNT incorporation is a promising way of broadening the use of this material. While the isotactic form is the most demanded in industry among polypropylene stereoisomers, syndiotactic polypropylene is also a promising material for film and fiber manufacturing [7], and nowadays its global production has reached a capacity of ~14 million kg/year [8].

The main obstacles in the way of developing advanced CNT-reinforced polymer composites are the problem of nanotube aggregation and the challenge of creating strong interface between filler particles and polymer matrix [9]. For the polyolefins that have non-polar chemical structure, efficient blending with inorganic fillers (particularly CNTs) is especially critical [10, 11]. A promising route to resolving these issues is the employment of in situ polymerization method [12–20], which involves ultrasonication for effective CNT dispersion and polymerization of monomer on nanotube surface that promotes intimate contact between polymer chains and nanotubes. Metallocene catalysts are the most efficient and versatile tool for obtaining polypropylene-based nanocomposites. Homogeneous metallocenes are

soluble in hydrocarbons, and therefore, they can perfectly cover the surface of nanoparticles and fibers [20, 21]. Moreover, metallocene catalysts provide unmatched opportunities for the precision synthesis of stereoregular polyolefin architectures and tailoring polymer matrix properties [22, 23].

In this paper we report about the novel technique for obtaining polypropylene/CNT nanocomposites based on in situ polymerization approach. According to our method, CNT dispersion and subsequent propylene polymerization are accomplished in a bulk of liquid monomer. Utilization of liquid propylene in such a way simplifies the process of nanocomposite synthesis, making it easily scalable for industrial application and ensures high rates of polymerization since monomer concentration in reaction medium is very high. Another advantage of this method is the total integration of all the experimental stages and components in the entire system. CNT dispersion via ultrasonication proceeds in the presence of a cocatalyst, methylaluminoxane (MAO). This leads to immobilization of MAO molecules on CNT surface mainly by loose ionic interactions and, to a lesser extent, by virtue of covalent bonding to –COOH or –OH groups, which are inherent to partially oxidized CNTs. The formation of catalytic active sites proceeds via heterogenization of the metallocene catalyst precursor on CNT surface owing to chemical interaction of metallocene with MAO directly during the initial stage of polymerization at lowered temperature.

Isotactic polypropylene (iPP) and syndiotactic polypropylene (sPP) nanocomposites reinforced with multi-wall carbon nanotubes (MWCNTs) have been synthesized. The present study embraces microstructure analysis of the obtained materials along with the characterization of their mechanical, electrical, and thermal properties.

## Experimental section

### Materials

Pristine CVD-grown MWCNTs (purity ≥95%, average diameter <10 nm, length range 5–15 μm) were purchased from Shenzhen Nanotech Port Co., Ltd., China (trade name of product is L-MWNTs-10). As-received MWCNTs were purified and mildly oxidized by boiling 30 wt.% nitric acid for 1 h with subsequent settling at room temperature for 20 h. This procedure was carried out in order to remove rest of amorphous carbon and impurities that might be poisonous for metallocene catalysts and to increase content of carboxylic and hydroxyl groups on MWCNTs. The acid-treated MWCNTs were filtered and washed repeatedly with deionized water, dried in vacuum at 400 °C for 5 h, and then stored in argon atmosphere. Polymerization grade propylene was provided by Moscow Oil Refining Plant and used in nanocomposite synthesis without any additional treatment. Isospecific $C_2$-symmetry metallocene catalyst *rac*-$Me_2Si(2\text{-Me-4-PhInd})_2ZrCl_2$ (MC-1) for iPP/MWCNT nanocomposite preparation was purchased from Boulder Scientific Co., and $C_s$-symmetry metallocene $Ph_2C(Cp)FluZrCl_2$ (MC-2) for obtaining sPP/MWCNT nanocomposites was synthesized in Moscow State University according to the technique described in literature [24]. MAO as a 10 wt.% solution in toluene was purchased from Witco and used as received. Metallocenes were used in the form of toluene solutions (0.01–0.03 wt.%) pre-activated with MAO. Polymerization experiments were carried out at 60 °C temperature and 2.5 MPa pressure in 200 $cm^3$ stainless steel autoclave reactor equipped with an internal sonotrode for MWCNT ultrasonication and a high speed mechanical stirrer (3,000 rpm). Reactor, containing required amount of MWCNTs, was evacuated for 1.5 h at 60 °C before polymerization experiments and then filled with 150 ml of liquid propylene and 2.5–5 g of 10 wt.% MAO solution. The pre-reaction mixture was then sonicated for 30 min with the use of 300 W 40 kHz ultrasonic generator. Polymerization assisted by mechanical stirring was started immediately after MWCNT ultrasonication by injecting metallocene solution into the precooled (10 °C for MC-1/MAO or 20 °C for MC-2/MAO) reactor to provide homogeneous distribution of active sites on MWCNT surface. After a 2-min initial stage of polymerization, the reaction temperature was raised to 60 °C. Polymerizations were carried out for 10–15 min (for iPP composites) or 15–35 min (for sPP materials) and then quenched by adding ethanol. After polymerization, the composite powder was extracted from the reaction mixture by simply depressurizing the unreacted propylene gas from the reactor.

Composition of the materials was controlled by adjusting 3 variables, namely, MWCNT weight, polymerization time, and metallocene amount. Catalyst amounts ranged between $3.0 \times 10^{-7}$ and $4.6 \times 10^{-7}$ mole for MC-1 and between $1.1 \times 10^{-6}$ and $1.6 \times 10^{-6}$ mole for MC-2. MAO/zirconium molar ratio was kept within the bounds of 12,000–14,000 for MC-1/MAO catalyst system and 4,500–7,000 for MC-2/MAO.

After polymerization quenching, the composites were placed for 24 h in ethanol acidified by hydrochloric acid in order to remove aluminum hydroxide and catalyst residues. After that, the materials were repeatedly washed with distilled water and ethanol, and then dried in vacuum at 40 °C.

### Characterization

Molecular weights and molecular weight distributions of the neat and MWCNT-filled polymers were evaluated by

GPC in a Waters 150C at 130 °C by using linear $\mu$-styragel HT columns and 1,2,4-trichlorobenzene as the eluent. The molecular weights were determined by employing polystyrene calibration curve as a reference.

The $^{13}C$ NMR spectra of the pure polymers and composites were recorded at 100 °C on a Bruker DPX-250 spectrometer operated at 62.895 MHz. The samples were prepared by dissolving polymer or composite powders in o-dichlorobenzene.

The uniaxial tensile testing of the nanocomposites was performed at room temperature (20 °C) on Instron 1,122 machine at 50 mm/min tensile speed. The film samples for mechanical testing were prepared by hot pressing of the nanocomposite powders at 190 °C and 10 MPa for 5 min and subsequent cooling at 16 K/min rate, and dog-bone specimens (with dimensions 35 × 5 × 0.5 mm) were cut from films. Multiple tests (5 for each material) were implemented for the reproducibility.

Morphology of fracture surfaces of the nanocomposite films was observed using Hitachi S-520 scanning electron microscope (SEM). Isotropic film samples prepared as mentioned above were fractured in liquid nitrogen and gold-sputtered prior to SEM imaging.

DC conductivity of the materials was measured by utilizing a two-probe method at room temperature for the film samples (0.5-mm-thick). Electrical properties of the polypropylene/MWCNT nanocomposites in microwave range (3.2–40 GHz) were evaluated by cavity resonance method using KSVN R-2 instruments (Russia) with rectangular-shaped resonators ($H_{0ln}$ operating mode). Cavity resonance method is based on the determination of resonance frequency change $\Delta f$ and the change of cavity $Q$-factor $(1/Q - 1/Q_0)$ when measured sample is inserted into the cavity. Direct measurements yield real ($\varepsilon'$) and imaginary ($\varepsilon''$) parts of nanocomposite permittivity.

Thermal conductivity of the materials was measured using heat flow method. Thermal conductivity coefficient ($\lambda$) was determined according to the following formula: $\lambda = (W - \Delta W) \times h/(T - \Delta T) \times S$, where $W$ is the power of heat source (W), $\Delta W$ is the heat loss to the environment (W), $h$ is the height of the measured sample (m), $T$ is temperature difference between heat source and heat receiver (K), $\Delta T$ is temperature loss at the edges of sample (K), and $S$ is the cross section of sample ($m^2$). Cylinder-shaped samples (dimensions: 15 mm diameter and 5 mm height) were prepared by hot pressing of the materials at 180 °C and 10 MPa and subsequent cooling with 7 K/min rate. Relative error in thermal conductivity measurements is ±10%.

DSC measurements were carried out on Perkin-Elmer DSC-7 differential scanning calorimeter at 10 K/min scanning rate for the nascent powder samples. Immediately after first heating run, the samples were cooled down and then heated again at the same rate (10 K/min). Results of the first cooling and of the second heating runs were taken into account. Thermogravimetry analysis (TGA) of the nascent composite powders was performed on Perkin-Elmer TGA-7 instrument in air atmosphere at 20 K/min heating rate.

## Results and discussion

### Nanocomposite synthesis results

iPP/MWCNT nanocomposites with filler loadings ranging from 0.1 to 3.5 wt.% and sPP/MWCNT nanocomposites containing 0.1–2.5 wt.% MWCNTs have been obtained by in situ polymerization method in liquid propylene medium. According to the composite synthesis peculiarities, metallocene active sites are assumed to be partly heterogenized on MWCNT surface, and partly distributed in solution in homogeneous state. Nevertheless, the composite powder examination provides clear evidence of efficient catalyst heterogenization achieved by propylene in situ polymerization: homogeneous grayish powders without visible traces of pure iPP or sPP have been obtained and noticeable reduction of reactor fouling (which takes place in the absence of filler) was observed. Prevention of reactor fouling in the presence of nanofiller has also been reported by Mulhaupt et al. for PE/boehmite nanocomposites prepared by in situ polymerization [25]. For iPP/MWCNT nanocomposites, dramatic transformation in powder morphology as compared to the neat iPP has been observed. Unlike gross grainy powders of the neat iPP (average diameter of grains is ~0.5 mm), iPP/MWCNT nanocomposite powders consist of very small fibril-like particles of submillimeter diameter. Bulk density considerably decreases from ~0.25 g/cm$^3$ for the neat iPP to ~0.07–0.09 g/cm$^3$ for the iPP/MWCNT powders. Nevertheless, sPP/MWCNT composites does not exhibit transformation in powder morphology in comparison with the pure sPP, and only color change from white to progressive gray depending on filler content takes place.

Activities of the catalytic systems plotted vs. MWCNT concentrations in reaction medium are presented in Fig. 1. Catalyst activity remains almost unchanged in the presence of MWCNTs either for MC-1/MAO (~100 kg iPP/(mmol Zr h)) or for MC-2/MAO (~30 kg sPP/(mmol Zr h)). Constancy of catalyst activity enables precision control of filler content in the composites.

Molecular weight of the neat iPP synthesized the identical conditions to the nanocomposites is $M_w$ ~600,000 ($M_w/M_n = 2.2$) and of the neat sPP is ~311,000 ($M_w/M_n = 2.0$). The influence of nanotube incorporation in polymerization medium on molecular weight and

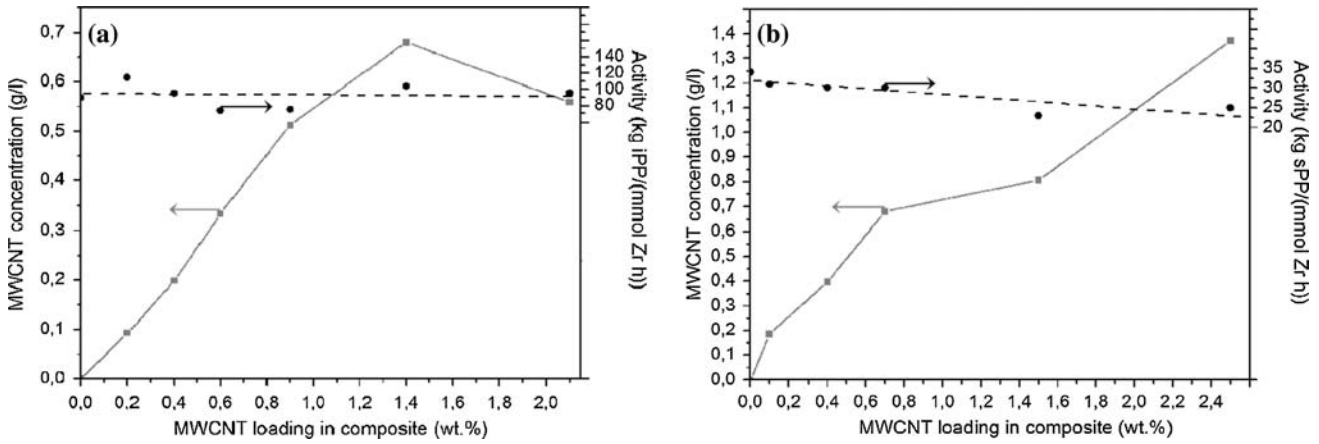


**Fig. 1** Catalyst activities at different MWCNT concentrations in liquid propylene corresponding to iPP/MWCNT nanocomposite synthesis (**a**) and sPP/MWCNT nanocomposite synthesis (**b**)

**Table 1** Molecular weight characteristics and tacticity of the pure sPP and MWCNT-filled sPP

| Sample | $M_w$ | $M_n$ | $M_w/M_n$ | rrrr (%) | mmrr (%) | mmrm + rrmr (%) | rmmr (%) |
|---|---|---|---|---|---|---|---|
| sPP | 310,800 | 153,900 | 2.01 | 91.58 | 3.46 | 1.76 | 1.33 |
| sPP/0.4 wt.% MWCNT | 307,500 | 136,500 | 2.25 | 90.99 | 3.64 | 2.46 | 1.66 |
| sPP/1.5 wt.% MWCNT | 271,900 | 122,000 | 2.22 | n.d. | n.d. | n.d. | n.d. |
| sPP/2.5 wt.% MWCNT | 279,300 | 133,400 | 2.09 | 94.03 | 3.45 | 1.17 | 1.35 |

stereoregularity of PP has been studied for the sPP/MWCNT system. Molecular weight characteristics of pure sPP and MWCNT-filled sPP determined by GPC and pentad distributions derived from $^{13}C$ NMR spectroscopy measurements are listed in Table 1. The corresponding data indicate that the introduction of MWCNTs in polymerization medium does not provoke noticeable change in MC-2 catalyst behavior: variations in molecular weight characteristics and tacticity are negligible and can be disregarded upon analyzing the evolution of sPP properties induced by nanotube loading.

## Microstructure of the nanocomposites

SEM analysis of iPP/MWCNT and sPP/MWCNT nanocomposite fracture surfaces reveals different filler dispersion efficiency achieved in various composite systems (Fig. 2). Both individual nanotubes and nanotube aggregates are present in iPP and sPP matrices, but much higher degree of CNT agglomerate exfoliation has been attained in iPP/MWCNT nanocomposites. While well-separated individual MWCNTs prevail in iPP/MWCNT materials, sPP-based composites exhibit strong filler aggregation. For the sPP/0.4 wt.% MWCNT sample, predominant formation of relatively compact nanotube clusters integrating 6–8 individual nanotubes takes place, but at filler contents higher than 1.5 wt.% strongly agglomerated CNT structures with micrometer dimensions are formed in sPP matrix. These microstructural features of the composites have strong connection with the materials properties that will be discussed below. Due to considerable nanotube aggregation, the sPP/MWCNT materials have substantially lower interfacial area as compared to the iPP/MWCNT nanocomposites that especially correlates with the electrophysical properties of the composites. We suppose that filler aggregation in the sPP/MWCNT composites is mostly related to the catalytic aspect of in situ polymerization. Previous studies on propylene polymerization kinetics conducted in comparable experimental conditions [26, 27] demonstrated that the rate of MC-2/MAO active sites formation is considerably lower in comparison with MC-1/MAO. Thus, it is assumed that coating of filler particles with polymer shells is delayed for the sPP/MWCNT composites as compared to the iPP/MWCNT, and nanotubes have more freedom to re-aggregate in the presence of MC-2 catalyst. Consequently, the catalytic peculiarities of in situ polymerization not only determine the productivity of composite synthesis and polymer matrix properties, but also have strong influence on nanotube dispersion.

## Mechanical properties

Noticeable mechanical reinforcement effect is observed in the iPP and sPP nanocomposites even upon incorporating

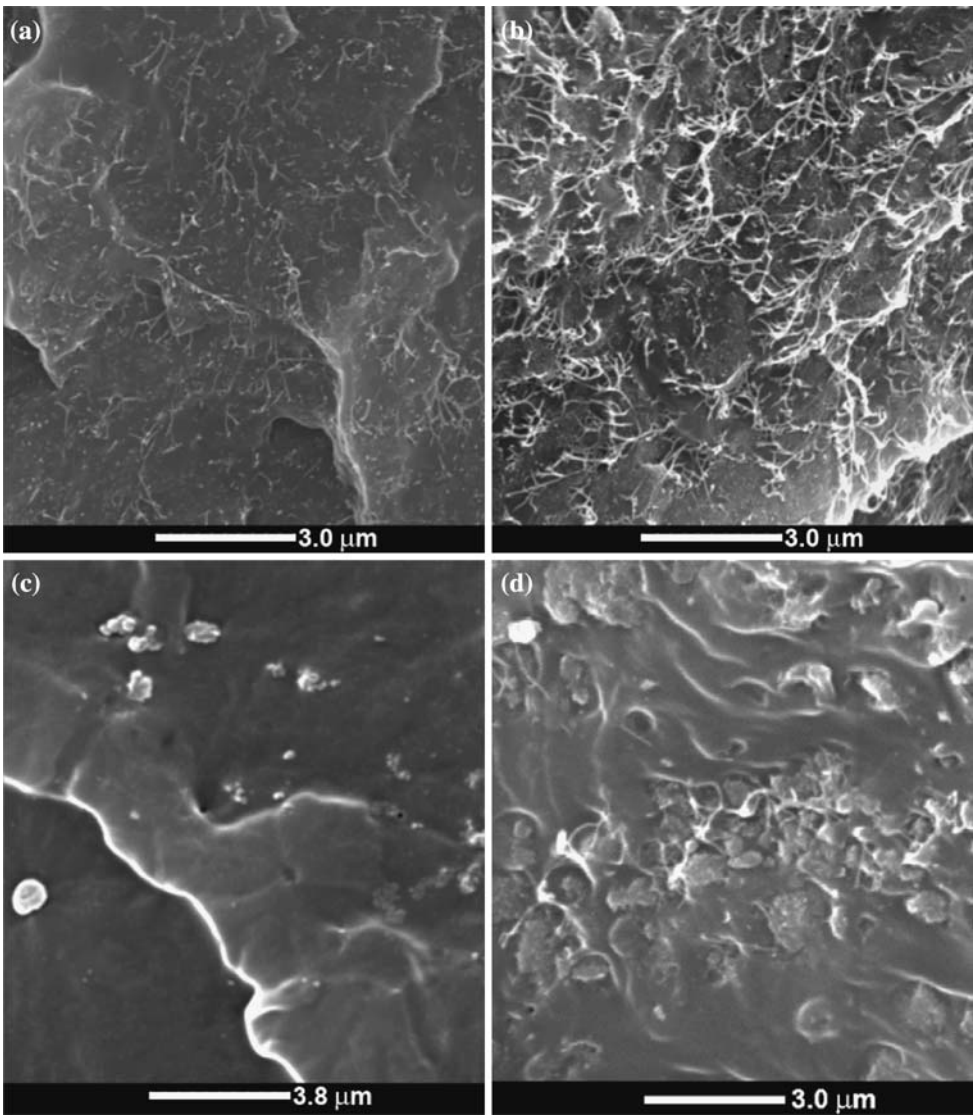


**Fig. 2** SEM images of the iPP and sPP nanocomposites: iPP/0.6 wt.% MWCNT (**a**), iPP/1.4 wt.% MWCNT (**b**), sPP/0.4 wt.% MWCNT (**c**), sPP/1.5 wt.% MWCNT (**d**)

lowest nanotube amount: at 0.1 wt.% MWCNT loading Young's modulus of iPP increases by ~22% from ~1,200 MPa to ~1,465 MPa, and modulus of sPP increases by ~34% from ~380 MPa to ~510 MPa (Fig. 3). Further modulus enhancement continues up at higher filler concentrations. Ultimate Young's modulus improvement of iPP is ~37% (from ~1,200 MPa to ~1,650 MPa) at 2.1 wt.% MWCNT content. Subsequent moderate modulus drop at 3.5 wt.% of MWCNTs is apparently connected with the nanotube agglomeration that is inevitable at such high CNT concentrations. For the sPP/MWCNT composites maximal mechanical reinforcement is achieved at 0.4 wt.% nanotube loading (Young's modulus grows by ~66% from ~380 MPa to ~635 MPa), and posterior modulus reduction at higher nanotube contents signifies considerable impact of MWCNT aggregation that takes place in this system.

Yield strength of the iPP/MWCNT and sPP/MWCNT composites varies slightly with filler content (Fig. 4) and indicates relatively low interfacial adhesion level in the materials. This is a typical behavior for the composites based on non-polar polyolefin matrices, whereas considerably higher adhesion and stronger interfaces have been attained for polar matrices [28–30]. The adhesion level achieved for the iPP/MWCNT and sPP/MWCNT composites is insufficient for substantial polymer reinforcement and is subject for improvement by nanotube functionalization.

## Electrical properties

DC conductivity measurements of the iPP/MWCNT and sPP/MWCNT nanocomposites show no percolation behavior within the investigated range of nanotube

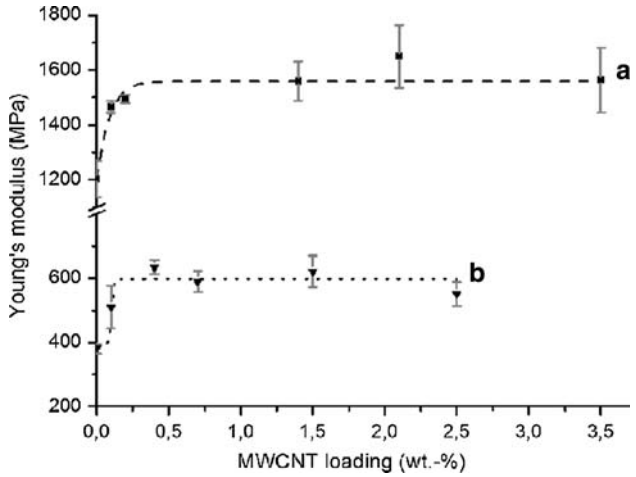


**Fig. 3** Young's modulus of iPP/MWCNT nanocomposites (a) and sPP/MWCNT nanocomposites (b) as a function of MWCNT loading

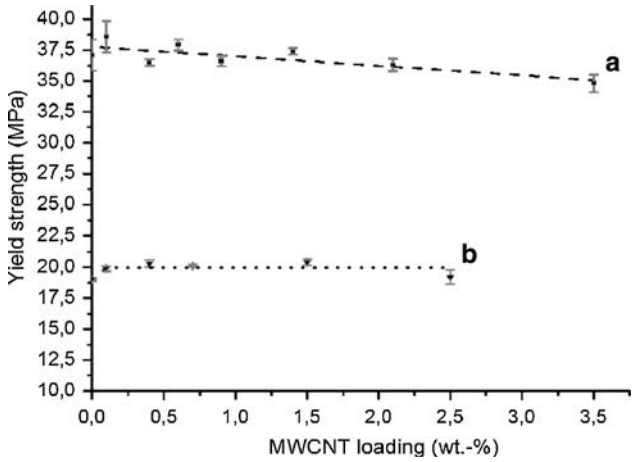


**Fig. 4** Correlations between yield strength and MWCNT content for iPP/MWCNT nanocomposites (a) and sPP/MWCNT nanocomposites (b)

loadings (up to 3.5 wt.%). Electrical resistivity of all materials exceeds $1 \times 10^{15}$ Ohm cm, the instrument's sensitivity threshold. It is in agreement with the literature data for polyethylene/MWCNT composites [31] for which percolation threshold at ca. 8 wt.% nanotube loading was reported. The absence of percolation transition is apparently owing to the lack of conductive paths in materials. For the iPP-based materials, this can be explained by perfect coating of filler particles with polymer shells achieved via in situ polymerization, and this point of view is also supported by the thermal conductivity data discussed below. However, imperfect exfoliation of MWCNT agglomerates is the most probable explanation for this fact for the sPP/MWCNT system.

Analyzing electrical properties of the materials in microwave range provides deep insight into the microstructural features of the synthesized PP/MWCNT composites. Microwave studies indicate conspicuous

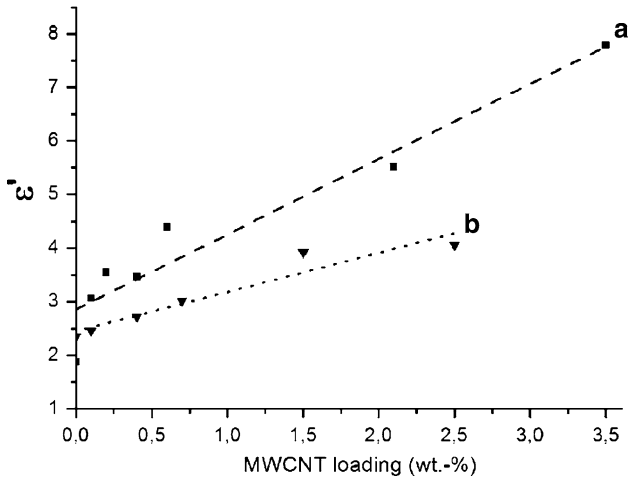


**Fig. 5** Permittivity at frequency 4.8 GHz as a function of filler loading for iPP/MWCNT nanocomposites (a) and sPP/MWCNT nanocomposites (b)

difference in the electrical properties of the iPP/MWCNT nanocomposites as compared to the sPP/MWCNT. Thus, the iPP/MWCNT nanocomposites exhibit considerably higher permittivity values in comparison with the sPP/MWCNT materials (Fig. 5). This behavior corresponds to different frequencies in microwave range. Slower growth of the sPP/MWCNT permittivity with increasing filler content is attributed to the nanotube agglomeration. The slope characterizing linear dependence between permittivity of composite and MWCNT concentration (Fig. 5) depends on the filler particles depolarization coefficient, which is determined by the aspect ratio of filler particles (length/diameter ratio for nanotubes). Analysis of these functional dependences has been performed with the use of the theoretical model described elsewhere [32]. Electrical properties of polymer composite systems containing spherical filler particles are adequately described by Bruggeman's equation up to 30 vol.% filler concentration: [33]

$$\frac{\varepsilon_f - \varepsilon}{\varepsilon_f - \varepsilon_m}\left(\frac{\varepsilon_m}{\varepsilon}\right)^{1/3} = 1 - v_f \tag{1}$$

Bruggeman's equation can be generalized for ellipsoidal filler shape: [34]

$$\frac{\varepsilon_f - \varepsilon}{\varepsilon_f - \varepsilon_m}\left(\frac{\varepsilon_m}{\varepsilon}\right)^{\alpha}\left(\frac{\varepsilon_f\beta + \varepsilon_m}{\varepsilon_f\beta + \varepsilon}\right)^{\gamma} = 1 - v_f, \tag{2}$$

where $\alpha = 3A(1 - 2A)/(2 - 3A)$, $\beta = (2 - 3A)/(1 + A)$, $\gamma = 2(3A - 1)/(1 + 3A)/(2 - 3A)$, $A = A_y = A_z$ is the depolarization coefficient.

The following equations were used to derive the functions $\varepsilon'(v_f)$ and $\varepsilon''(v_f)$, suitable for the description of composites containing elongated filler particles (i.e., nanotubes) [34]:

$$\varepsilon = \varepsilon_m + \frac{v_f}{3}\sum_1^3 \frac{\varepsilon_f - \varepsilon_m}{1 + A_i(\varepsilon_f/\varepsilon_m - 1)} \quad (3)$$

$$\varepsilon = \varepsilon_m + \frac{v_f}{3(1 - v_f)}\sum_1^3 \frac{\varepsilon_f - \varepsilon_m}{1 + A_i(\varepsilon_f/\varepsilon_m - 1)} \quad (4)$$

where $\varepsilon$ is the complex dielectric constant, and $A_i$ are the depolarization coefficients. Depolarization coefficients for prolate ($l > d$) ellipsoids in uniform electric field were taken from [35]:

$$A_x = \frac{1 - e^2}{e^3}(\text{arth}(e) - e),\ A_y = A_z = (1 - A_x)/2,$$
$$e = \sqrt{1 - d^2/l^2} \quad (5)$$

Dielectric losses of filler were calculated to be

$$\varepsilon'' = i\kappa\lambda\sigma, \quad (6)$$

where $\kappa = 1/(2\pi c\varepsilon_o)$, $\sigma$ is the conductivity of fibers, $\lambda$ is the wavelength, and $\varepsilon_0$ is the vacuum permittivity.

The following minor parameters were used: $v = \varepsilon_m/\varepsilon_f \ll 1$ and $\mu = d/l \ll 1$ (conductivity of the matrix is negligible compared to that of filler). It follows from Eq. 5 that if $\mu \ll 1$, then $A_x \ll 1$ is also a minor parameter. Equations 3 and 4 were expanded over parameters $v$ and $A_x$ and, using Eqs. 5 and 6, the following expressions were derived:

$$\varepsilon = \varepsilon_m + \frac{v_f\varepsilon_m/3A_x}{1 - i\varepsilon_m/\kappa\lambda\sigma A_x} \quad (7)$$

$$\varepsilon = \varepsilon_m + \frac{v_f}{1 - v_f}\frac{v_f\varepsilon_m/3A_x}{1 - i\varepsilon_m/\kappa\lambda\sigma A_x} \quad (8)$$

Separating real and imaginary parts of Eq. 8, one can write:

$$\varepsilon' = \varepsilon_m + \frac{v_f}{1 - v_f}\frac{\varepsilon_m/3A_x}{1 + (\varepsilon_m/k\lambda\sigma A_x)^2} \quad (9)$$

$$\varepsilon'' = \frac{v_f}{1 - v_f}\frac{\varepsilon_m^2/3k\lambda\sigma A_x^2}{1 + (\varepsilon_m/k\lambda\sigma A_x)^2} \quad (10)$$

Equation 9 was fitted to experimental data with $A_x$ as a parameter. Then Eq. 5 was used to estimate relative filler aspect ratios for the iPP/MWCNT and sPP/MWCNT systems. As a result, the approximate nanotube aspect ratio for the iPP/MWCNT nanocomposites is ~25, and for the sPP/MWCNT it is ~10. These values obtained from microwave electrical measurements only roughly correspond to the actual CNT aspect ratios in synthesized materials and can be used only for the relative comparison of nanotube aspect ratios in two systems. Accordingly, we can conclude about the formation of lesser anisotropic MWCNT clusters in the sPP/MWCNT composites with diameter ~2.5 times higher as compared to those in iPP/MWCNT nanocomposites. Thus, microwave electrical analysis provides easy solution for studying nanotube agglomeration in various composite systems and their comparison.

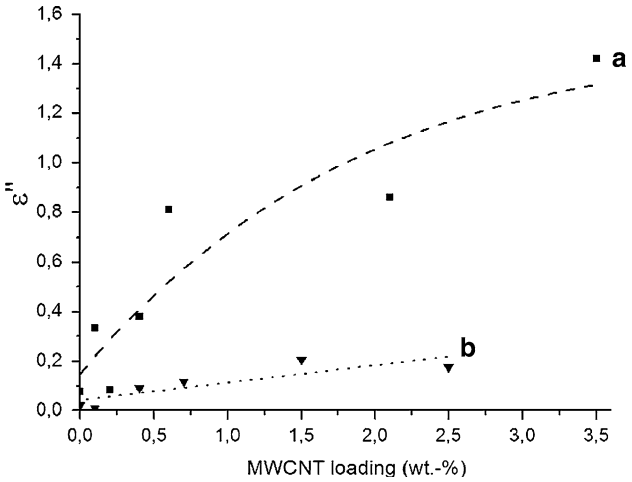


**Fig. 6** Dielectric losses at 4.8 GHz as a function of filler loading for iPP/MWCNT nanocomposites (a) and sPP/MWCNT nanocomposites (b)

Dielectric loss factor of the materials also correlates with the interfacial area in the composites. Consequently, the iPP/MWCNT nanocomposites exhibit higher dielectric losses in the comparison with the sPP/MWCNT materials (Fig. 6). High dielectric losses in microwave range for the iPP/MWCNT nanocomposites indicate substantial energy dissipation within the materials. Due to relatively low permittivity values and considerable dielectric losses, the respective nanocomposites can find use as efficient electromagnetic shielding materials and microwave absorbing filters—it is an example of non-conductive materials that however utilize the potential of conductive filler particles in a high frequency range.

## Thermal properties

Incorporation of MWCNTs in iPP and sPP by in situ polymerization induces only minor improvement in thermal conductivity of the polymers (up to 10% at 3.5 wt.% filler concentration) (Fig. 7). Apparently, it is a result of efficient coating of filler particles with insulating polymer shells that create high thermal resistance at PP/nanotube interface, thus hindering phonon mobility in the studied systems. High interfacial thermal resistance is considered as the main factor restricting thermal conductivity in composites [36] and severely diminishes intrinsically outstanding thermal conductivity of CNTs.

Melting temperatures, fusion enthalpies and crystallization temperatures of the iPP/MWCNT and sPP/MWCNT nanocomposites are listed in Table 2. The incorporation of MWCNTs in iPP and sPP matrices has moderate impact on the fusion enthalpy ($\Delta H_m$) of the polymers: we observe certain growth of this parameter that indicates slight increase in the polymer crystallinity, but there is no definite correlation between $\Delta H_m$ and nanotube loading. It is worthy of note

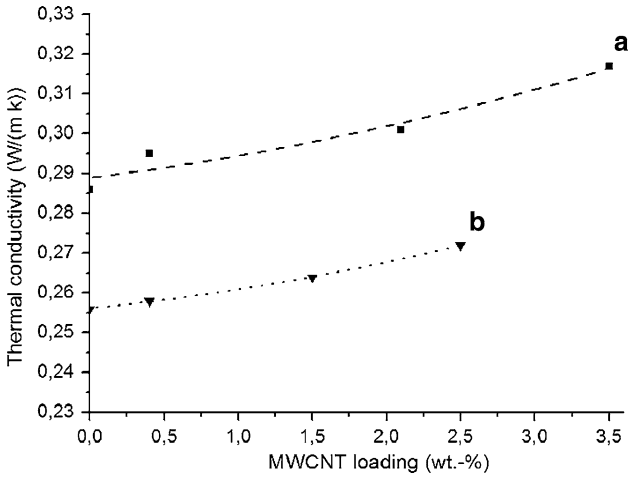


**Fig. 7** Thermal conductivity of iPP/MWCNT nanocomposites (a) and sPP/MWCNT nanocomposites (b)

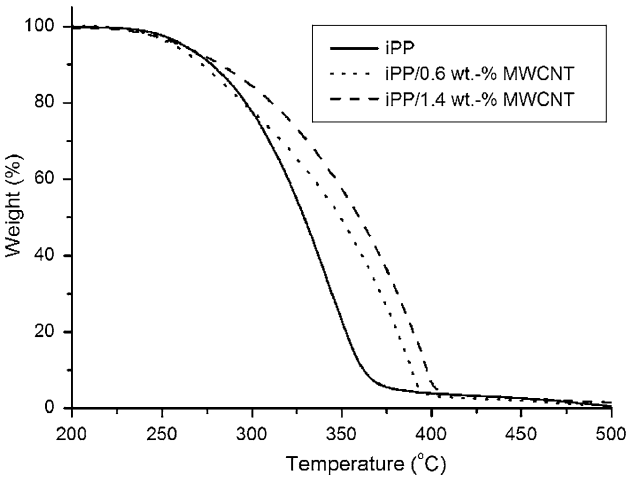


**Fig 8** TGA profiles of iPP/MWCNT nanocomposites

**Table 2** Melting temperatures, fusion enthalpies, and crystallization temperatures of iPP/MWCNT and sPP/MWCNT nanocomposites

| Material | $T_m$ (°C) | $\Delta H_m$ (J/g) | $T_c$ (°C) |
|---|---|---|---|
| iPP | 156.6 | 90.7 | 108.9 |
| iPP/0.1 wt.% MWCNT | 156.3 | 97.2 | 112.7 |
| iPP/0.4 wt.% MWCNT | 157.1 | 92.2 | 117.1 |
| iPP/0.6 wt.% MWCNT | 157.6 | 97.3 | 115.6 |
| iPP/0.9 wt.% MWCNT | 158.5 | 95.8 | 116.2 |
| iPP/1.4 wt.% MWCNT | 158.1 | 93.7 | 122.5 |
| iPP/2.1 wt.% MWCNT | 157.6 | 93.4 | 121.0 |
| iPP/3.5 wt.% MWCNT | 157.5 | 94.8 | 122.7 |
| sPP | 131.5 | 44.1 | 91.1 |
| sPP/0.1 wt.% MWCNT | 137.6 | 51.6 | 109.2 |
| sPP/0.4 wt.% MWCNT | 134.5 | 48.4 | 108.2 |
| sPP/0.7 wt.% MWCNT | 138.1 | 49.5 | 109.2 |
| sPP/1.5 wt.% MWCNT | 134.1 | 47.1 | 107.9 |
| sPP/2.5 wt.% MWCNT | 134.1 | 46.3 | 90.2 |

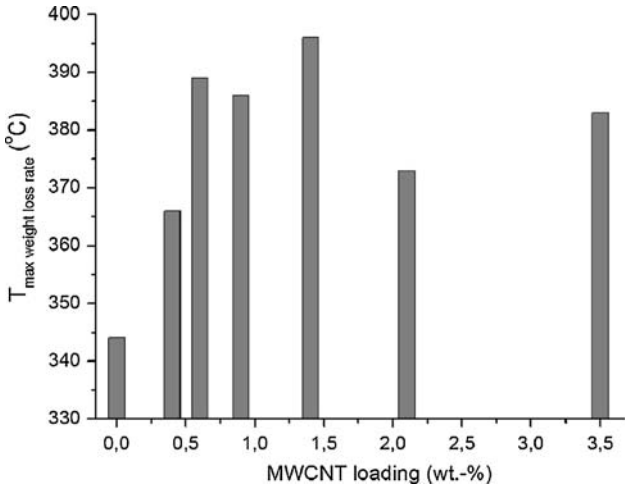


**Fig. 9** Maximal weight loss rate temperatures for the iPP/MWCNT nanocomposites extracted from TGA profiles

that sharpest $\Delta H_m$ growth takes place at lowest MWCNT loading (0.1 wt.%) either for iPP or for sPP, and this factor can contribute to the abrupt increase in the Young's modulus of the composites. Carbon nanotubes exert evident influence as nucleating agents causing the rise of iPP and sPP crystallization temperature ($T_c$). The achieved marked improvement in polymer crystallization behavior is favorable for the processing of the materials, and for sPP it is the subject of particular interest, since its application is severely limited owing to the low crystallization temperature and low crystallization rate [37]. The marked decrease of $T_c$ for sPP/2.5 wt.% MWCNT composite as compared to the sPP-based composites with lower nanotube loadings is obviously related to the strong MWCNT agglomeration at this filler content and the corresponding decrease of the number of crystallization sites in the polymer.

Thermal oxidative degradation of the iPP and iPP/MWCNT nanocomposites has been investigated by employing TGA analysis in air atmosphere. TGA profiles of the materials are presented in Fig. 8. By differentiating TGA profiles, maximal weight loss rate temperatures for the nanocomposites were extracted and plotted in Fig. 9. Even low MWCNT concentrations led to notable retardation of iPP thermal oxidative degradation process. Upon introducing only 1.4 wt.% MWCNT, strong stabilization effect has been achieved: maximal weight loss rate temperature increases by ~52 °C as compared to the neat polymer. This thermal oxidative stabilization effect is mostly connected with the formation and stabilization of CNT-bonded macroradicals and nanotube barrier effect, implying hindered transport of polymer decomposition products within a volume of composite [38–40].

## Conclusion

The reported method for the synthesizing polypropylene/MWCNT nanocomposites via in situ polymerization demonstrates high potential for the production of new polypropylene-based advanced materials. The obtained results show that the catalytic peculiarities of in situ polymerization not only determine the productivity of composite synthesis and polymer matrix properties, but also have strong influence on nanotube dispersion. This fact indicates particular complexity in analyzing nanocomposite properties due to the specific details of materials synthesis, and in situ polymerization approach is puzzling greatly owing to a lot of variables involved. Our further investigation will be focused on nanocomposite properties optimization: the present results show that additional efforts are needed to provide high interfacial adhesion and enhanced polymer reinforcement. Carbon nanotube sidewall functionalization with short alkyl chains is a promising strategy for improving compatibility between PP matrix and filler particles.

**Acknowledgements** The authors gratefully thank Dr. Anastasia Bolshakova from Moscow State University for the assistance in SEM observations and Dr. Konstantin Bryliakov (G. K. Boreskov Institute of Catalysis, Siberian Branch of the Russian Academy of Sciences, Novosibirsk) for $^{13}C$ NMR analysis. The authors are also grateful to Professor Dmitry Lemenovsky and his group from Department of Chemistry of Moscow State University for the provision of the catalyst. This work was supported by Haldor Topsoe A/S grant.

## References

1. Ajayan PM (1999) Chem Rev 99:1787
2. Szleifer I, Yerushalmi-Rozen R (2005) Polymer 46:7803
3. Velasco-Santos C, Martinez-Hernandez AL, Castano VM (2005) Compos Interface 11(8–9):567
4. Moniruzzaman M, Winey KI (2006) Macromolecules 39:5194
5. Galli P, Vecellio G (2004) J Polym Sci [A1] 42:396
6. Balow MJ (2003) In: Karian HG (ed) Handbook of polypropylene and polypropylene composites. CRC Press, New York
7. Supaphol P, Spruiell JE (1999) In: Bendikt GM (ed) Metallocene technology in commercial applications. William Andrew Inc., Society of Plastics Engineers
8. Schwerdtfeger ED, Miller SA (2007) Macromolecules 40:5662
9. Ajayan PM, Tour JM (2007) Nature 447:1066
10. McIntosh D, Khabashesku VN, Barrera EV (2006) Chem Mater 18:4561
11. Maier C, Calafut T (1998) Polypropylene: the definitive user's guide and databook. William Andrew Inc., Plastics Design Library
12. Velasco-Santos C, Martinez-Hernandez AL, Fisher FT, Ruoff R, Castano VM (2003) Chem Mater 15:4470
13. Philip B, Xie J, Abraham JK, Varadan VK (2005) Polym Bull 53:127
14. Wiemann K, Kaminsky W, Gojny FH, Schulte K (2005) Macromol Chem Phys 206:1472
15. Kaminsky W, Wiemann K (2006) Compos Interface 13(4–6):365
16. Kaminsky W, Funck A, Wiemann K (2006) Macromol Symp 239:1
17. Funck A, Kaminsky W (2007) Composites Sci Tech 67(5):906
18. Bonduel D, Bredeau S, Alexandre M, Monteverde F, Dubois P (2007) J Mater Chem 17:2359
19. Bredeau S, Boggioni L, Bertini F, Tritto I, Monteverde F, Alexandre M, Dubois P (2007) Macromol Rapid Commun 28:822
20. Kaminsky W, Funck A (2007) Macromol Symp 260:1
21. Kaminsky W (2008) Macromol Chem Phys 209:459
22. Coates GW (2002) J Chem Soc Dalton Trans 467
23. Resconi L, Cavallo L, Fait A, Piemontesi F (2000) Chem Rev 100:1253
24. Razavi A, Atwood JL (1993) J Organomet Chem 459:117
25. Xalter R, Halbach TS, Mulhaupt R (2006) Macromol Symp 236:145
26. Nedorezova PM, Tsvetkova VI, Aladyshev AM, Savinov DV, Klyamkina AN, Optov VA, Lemenovskii DA (2001) Polym Sci Ser A 43(4)356
27. Nedorezova PM, Shevchenko VG, Shchegolikhin AN, Tsvetkova VI, Korolev YM (2004) Polym Sci Ser A 46(3)242
28. Liu T, Phang IY, Shen L, Chow SY, Zhang W-D (2004) Macromolecules 37:7214
29. Gao J, Itkis ME, Yu A, Bekyarova E, Zhao B, Haddon RC (2005) J Am Chem Soc 127:3847
30. Moniruzzaman M, Chattopadhyay J, Billups WE, Winey KI (2007) Nano Lett 7(5):1178
31. McNally T, Potschke P, Halley P, Murphy M, Martin D, Bell SEJ, Brennan GP, Bein D, Lemoine P, Quinn JP (2005) Polymer 46:8222
32. Ponomarenko A, Shevchenko V, Figovsky OL (2005) Scientific Israel—Technological Advantages 7:37
33. Scarisbrick RM (1973) J Phys D Appl Phys 6:2098
34. Reynolds JA, Hough JM (1957) Proc Phys Soc 70(8)425B:769
35. Landau LD, Lifshitz EM, Pitaevskii LP (1984) Electrodynamics of continuous media (course of theoretical physics), 2nd edn, vol 8. Elsevier Butterworth-Heinemann, Oxford
36. Huxtable ST, Cahill DG, Shenogin S, Xue L, Ozisik R, Barone P, Usrey M, Strano MS, Siddons G, Shim M, Keblinski P (2003) Nat Mater 2:731
37. Dotson DL (2003) WO 03/087175
38. Watts PCP, Fearon PK, Hsu WK, Billingham NC, Kroto HW, Walton DRM (2003) J Mater Chem 13:491
39. Raravikar NR, Schadler LS, Vijayaraghavan A, Zhao Y, Wei B, Ajayan PM (2005) Chem Mater 17:974
40. Marosfoi BB, Szabo A, Marosi G, Tabuani D, Camino G, Pagliari S (2006) J Therm Anal Cal 86(3):669